J Mater Sci: Mater Med (2009) 20:1047–1055
DOI 10.1007/s10856-008-3673-1

Fluoridated hydroxyapatite/titanium dioxide nanocomposite coating fabricated by a modified electrochemical deposition

Jian Wang · Yonglie Chao · Qianbing Wan · Kangping Yan · Yukun Meng

Received: 28 September 2008 / Accepted: 15 December 2008 / Published online: 30 December 2008

Abstract Fluoridated hydroxyapatite/titanium dioxide nanocomposite coating was successfully fabricated by a modified electrochemical deposition technique. F^- ions, nanoscaled TiO_2 particles and 6% H_2O_2 was added into the electrolyte, and ultrasonication was also performed to prepare this nanocomposite coating. The microstructure, phase composition, dissolution rate, bonding strength and in vitro cellular responses of the composite coating were investigated. The results show that the composite coating was uniform and dense owing to the effects of H_2O_2 and ultrasonication. The thickness of the composite coating was ~5 μm and scanning electron microscopy revealed that nanoscaled TiO_2 particles were imbedded uniformly between FHA crystals. The addition of F^- and TiO_2 reduced the crystallite size and increased the crystallinity of HA in FHA/TiO_2 composite coating. In addition, the composite coating shows higher bonding strength and lower dissolution rate than pure HA coating, and the in vitro bioactivity of FHA/TiO_2 composite coating was not affected as compared with pure HA coating.

J. Wang
State Key Laboratory of Oral Diseases, Sichuan University, Chengdu 610041, China

J. Wang · Y. Chao · Q. Wan (✉) · Y. Meng
Department of Prosthodontics, West China hospital of Stomatology, No. 14 of Sect. 3, People's Road South, Chengdu, Sichuan 610041, China
e-mail: fero@tom.com

K. Yan
School of Chemical Engineering, Sichuan University, Chengdu 610041, China

1 Introduction

Hydroxyapatite (HA) [$Ca_{10}(PO_4)_6(OH)_2$] is the primary mineral content, representing 43% by weight, of bone. Applying a thin layer of HA, to the surface of a metal implant, can promote osseointegration and increase the mechanical stability of the implant [1, 2]. The plasma spray technique is currently used to fabricate HA coatings, but the unavoidable HA decomposition due to a high-temperature process is the major problem of this method [3, 4]. Electrochemical deposition of HA coating has recently attracted considerable attention because of a variety of advantages of the method such as a low process temperature, the ability to deposit on porous or complex shapes of the substrate, the crystallinity of deposits increases with the electrolyte temperature, and the morphology of coating can be controlled easily by varying the electrochemical potential and electrolyte concentration [5–8].

However, previous studies revealed several major drawbacks which could limit the application potential of electrochemical method. Firstly, pure HA coating suffers relatively high dissolution rate in simulated body fluid that affects its long-term stability [9, 10]. Secondly, electrochemical reaction includes the reduction of water on the surface of the substrate, which will result in the formation of a large amount of H_2. H_2 gas will occupy the active surface sites and inhibit the precipitation of HA coating [11]. Thirdly, the bonding strength of HA coating produced by the electrochemical deposition is much lower than that by the plasma spray method [12].

To overcome these problems in traditional electrochemical deposition, several attempts have been made in this research, accordingly. First of all, NaF powder was added into the electrolyte in order to incorporate F^- ions

into the apatite structure of HA crystals and obtain fluoridated hydroxyapatite ($Ca_{10}(PO_4)_6F_x(OH)_{2-x}$, FHA, $0 < x < 2$) coatings. Fluorine is one of the trace elements in bone tissue and teeth of human bodies, and F^- is smaller than OH^-, therefore, the stability of HA can be improved and the dissolution rate can be decreased by substituting F^- for OH^- over a wide range of concentrations [13]. Furthermore, F^- promotes the mineralization and crystallization of calcium phosphate in the bone forming process [14]. Simultaneously, 6% H_2O_2 (mass fraction) was added into the electrolyte and ultrasonication was also performed during the deposition process. H_2O_2 can substitute H_2O to be reduced and change the mechanism of electrochemical reaction. The H_2 evolution may be erased and dense coatings may also deposit on Ti substrate at a weaker polarization potential after H_2O_2 is added into the electrolyte. Ultrasonication may also detach H_2 bubbles from the substrate surface and promote the formation of dense and uniform coatings [15]. Moreover, in order to increase the bonding strength of HA coating, nano-scaled TiO_2 particles were also added into the electrolyte to fabricate a composite coating. The incorporation of bioinert ceramics as reinforcement within the coatings is believed to be a way to improve the mechanical reliability of the HA matrix [16, 17]. In addition, it has been found that the addition of Ti, TiO_2 or ZrO_2 into HA had a major effect on the HA structure and a positive effect on HA properties [18, 19]. For example, TiO_2 is capable of enhancing osteoblast adhesion and inducing cell growth [20]. As for the process of electrochemical codeposition, Guglielmi [21] proposed two successive adsorption steps for the metal/inert particles composite coating prepared by electrochemical codeposited. According to Guglielmi's proposal, the first step is called loose adsorption in that there is a layer of adsorbed ions and solvent molecules screening the interaction between the electrode and the particles. The second step is a strong adsorption that is thought assisted by the electric field, whereby a substantial electrochemical reaction produces strong particle adsorption onto the electrode.

The aim of this study is to fabricate FHA/TiO_2 nanocomposite coatings by a modified electrochemical deposition technique. F^- ions, nanoscaled TiO_2 particles and 6% H_2O_2 was added into the electrolyte, and ultrasonication was also performed to prepare this nanocomposite coating. It is expected that a synergistic effect of codeposition of FHA and TiO_2 might exhibit improved bonding strength, chemical stability, and coating properties. The microstructure, phase composition, dissolution rate, bonding strength and in vitro cellular responses of the composite coatings were also investigated.

2 Materials and methods

2.1 Deposition of FHA/TiO_2 composite coatings by a modified electrochemical technique

Commercially pure titanium sheets (10 × 10 × 0.6 mm, Non-ferrous metals corporation, Baoji, China) were used as substrates for electrodeposition. Their surfaces were ground with #100 and #600 SiC paper, etched in 4% HF solution for 2 min, ultrasonicated in acetone and ethyl alcohol for 15 min, respectively, rinsed in double-distilled water, and finally dried. The edges of the titanium substrates were rounded to avoid an edge effect during electrodeposition.

The electrolyte used for deposition of coatings contained 0.042 M $Ca(NO_3)_2$, 0.025 M $NH_4H_2PO_4$, 0.15 M $NaNO_3$ and 6% H_2O_2 (mass fraction). $NaNO_3$ was added to improve the ionic strength of the electrolytes. For the fabrication of FHA/TiO_2 composite coatings, NaF ($[F^-] = 0.012$ M) and 0–50 g/l nanoscaled TiO_2 (typical size < 80 nm, Jiankun Chemical Reagent Corporation, Hefei, China) was added into the electrolyte. In order to keep TiO_2 particles dispersed in the electrolyte, ultrasonication with output frequency of 25 kHz was performed. The electrolyte was prepared with analytical reagent grade chemicals (Kelong Chemical Reagent Corporation, Chengdu, China) and deionized water. The pH of the electrolyte was adjusted to 6.0 at 25°C.

The coating process was carried out at 65°C in a conventional electrolytic cell fitted with a graphite rod acting as counter-electrode. An electric heater and magnetic agitation (Electrical Appliances Co. Changzhou, China) was used to maintain the temperature of electrolyte and stir the electrolyte at a speed of 180 rpm. The deposition was carried out in galvanostat mode and the cathodic current density was maintained at 0.6 mA/cm^2 for 120 min.

After deposition, the specimens were rinsed in distilled water, soaked in 0.1 M NaOH solution at 60°C for 48 h and finally calcined in vaccum at 650°C (heating rate = 5°C/min, maintaining time = 2 h, and cooling rate = 1°C/min). Compared with FHA/TiO_2 composite coating, pure HA and FHA coatings were designated as control.

The content of TiO_2 particles in composite coatings was measured gravimetrically by dissolving the coatings in diluted hydrochloride acid, filtering through weighted membrane filter paper and then calculating volume percent of TiO_2 in the coatings.

2.2 Coating characterization

The surface microstructures of the coatings were observed using a scanning electron microscopy (SEM, JEM-5900LV, JEOL, Tokyo, Japan). The specimens were coated with a conductive layer of carbon in a sputter coater to avoid charging effects. The elements were scanned for

quantitative analysis with X-ray photoelectron spectroscope (XPS, PHI 5600, Physical Electronics) using monochromatic Al K_α X-ray source. An X-ray diffraction instrument (XRD, D/max-rA, Rigaku Co. Japan) was used to analyze the crystal structure of the coatings. All samples were exposed to X-rays generated from a CuK_α source operating at 42 kV and 110 mA. Data were collected from $2\theta = 10°$ to 70° at 0.02° intervals with a 3-s data collection time for each angular increment. Flourier transform infrared spectroscopy (FT-IR, MX-1E, Nicolet Co.) was adopted to measure the oscillation spectrum of radical hydrogen phosphate, radical phosphate and hydroxyl.

2.3 Bonding strength test

The interfacial shearing strength of the coatings was tested using a Universal Instron Mechanical Testing System (Instron 5569, Instron Co.) according to ASTM F1044-05 standard [22]. This test relies on a bonding agent to remove the film with an applied shear strength. In this study, the coating surface of the 10 × 10 mm specimen was bonded to another metal surface with epoxy adhesive. The loading was applied in in-plane direction with crosshead speed of 10 mm/min. For each testing material, five specimens were used, and the bonding strength data were reported as the average value.

2.4 Dissolution test

In order to observe the dissolution behavior of the coatings, the specimens were immersed in citric acid modified phosphate buffer solution (CPBS) [23] for predetermined periods of time. The composition of CPBS was listed in Table 1. At the end of each incubation period, the weights of the coatings before and after soaking were obtained by an analytical balance (AB204-S, Mettler-Toledo Co. Zurich, Switzerland) with accuracy of ±0.1 mg.

2.5 In vitro cellular assessment

The cellular responses to the coatings were assessed in terms of the cell proliferation and alkaline phosphatase (ALP) activity [24]. The MC3T3-E1 osteoblast-like cell line was cultured on each specimen for up to 7 days at a seeding density of 1×10^4 cells/ml. Uncoated titanium substrate was tested for the purpose of comparison. Following the incubation, the cells were detached with a trypsin-EDTA solution and the living cells were counted using a haemocytometer (Superior Co. Germany). In order to observe the cell morphology after proliferation, SEM was performed after fixing the cells with 2.5% glutaraldehyde, dehydrating them with graded ethanol (70%, 90%, and 100%), and critical point drying in CO_2. The ALP activity was measured using the phosphate detection kit (BIOMOL GREEN, USA). All the experimental processes were conducted strictly according to the provided protocol. By using the microplate assay mode, the measurements were read at 620 nm in a microplate reader and the ALP activities were calculated from a standard curve.

Table 1 The composition of CPBS

Chemical (g/l)	NaCl	KCl	$Na_2HPO_4 \cdot 2H_2O$	KH_2PO_4	Citric acid
pH = 4.70	8	0.2	2.9	0.2	1.05
pH = 6.95	8	0.2	2.9	0.2	0.21

3 Results and discussion

3.1 Phase composition

Figure 1 compares the XRD patterns of HA, FHA and FHA/TiO_2 composite coatings after post-treatment process. Typical apatite peaks were observed in all patterns. The peak intensity of FHA was a little greater than that of HA and the peak width was a little narrower, indicating better crystallization and higher purity. It was revealed that F^- ions were favorable for the crystallization of apatite and the incorporation of F^- into the apatite structure resulted in smaller and denser crystals [25]. Moreover, the position of (300) peak of FHA coating shifted to a higher diffraction angle compared with that of HA coating because *a*-axis

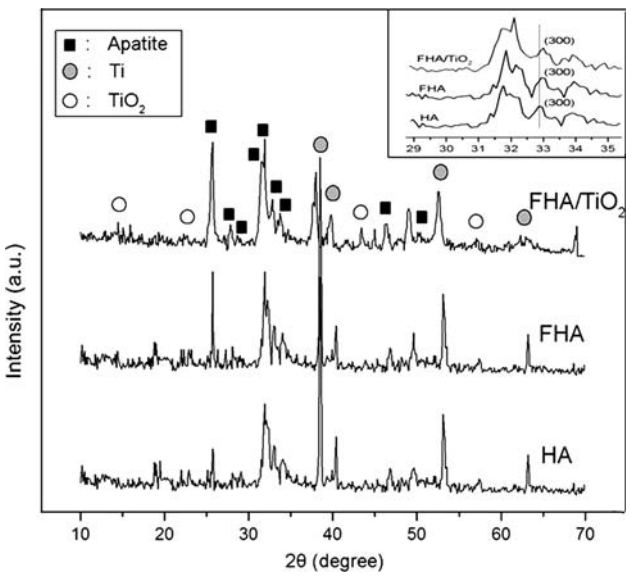

Fig. 1 XRD patterns of HA, FHA and FHA/TiO_2 composite coatings. Inset shows the short-range XRD patterns of all the coatings. It can be seen that (300) peaks of FHA and FHA/TiO_2 coatings shifted to a higher diffraction angle compared with that of HA coating

parameter in HA crystal reduced with the incorporation of F^- into the apatite structure. For FHA/TiO_2 composite coating, diffraction peaks due to FHA and anatase TiO_2 were observed without other phase being detected, which indicates that the presence of TiO_2 did not interfere with the FHA phase. The peak intensity of FHA/TiO_2 coating was higher than FHA coating, which means that the composite coating had smaller crystal size and higher crystallinity than either HA or FHA coating.

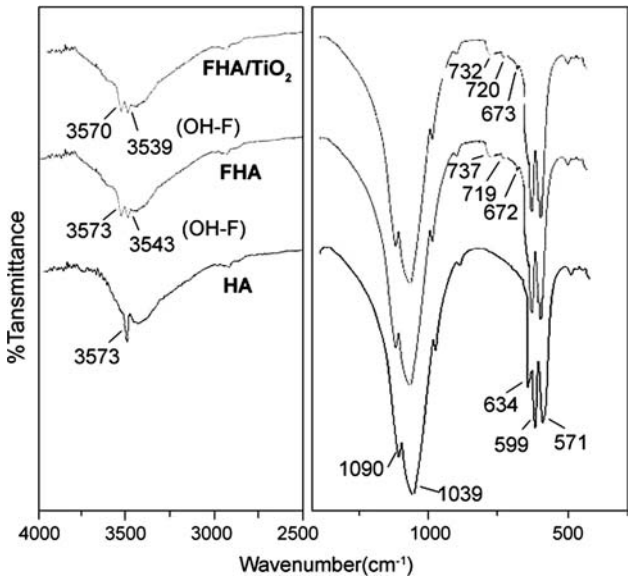

Fig. 2 FT-IR spectra of HA, FHA and FHA/TiO_2 coatings

The FTIR spectra of HA, FHA and FHA/TiO_2 composite coating are given in Fig. 2. For all the specimens, the vibration bands showed typical apatite characteristics, with PO_4^{3-} bands at around 1090, 1039, 599 and 571 cm^{-1}. The bands observed at 3570 and 633 cm^{-1} were assigned to free OH^- stretching and wagging, respectively. The hydroxyl stretching peaks at 3570 cm^{-1} for FHA and FHA/TiO_2 coatings split and an additional OH–F stretching band appeared at a lower frequency, signifying the substitution of F^- for OH^-. It was also found that new peaks appeared around 674 and 720 cm^{-1} when F^- was incorporated into the apatite coatings.

Figure 3 shows the XPS spectra of HA, FHA and FHA/TiO_2 coatings. For FHA and FHA/TiO_2 coatings, F1s peak was evident in the wide scan and the narrow scan analysis revealed only one peak at ~684.3 eV belonging to F1s. That peak is the fingerprint for fluorine in FHA structures [26]. Moreover, the contents of Ca, F, and P in the coatings were determined by ratio of the area under the respective elemental peak in the XPS narrow scan spectrum, and the results were tabulated in Table 2. As indicated in the table, the measured Ca/P ratio was in the range of 1.61–1.64, close to the stoichiometric value of 1.67, which means

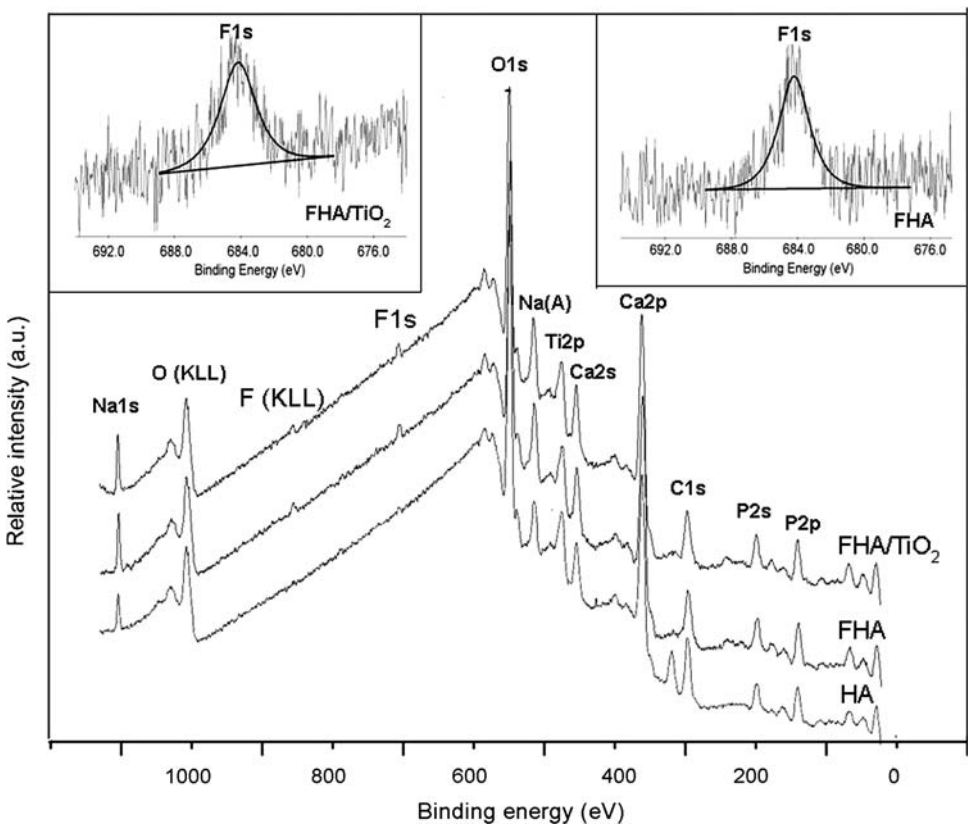

Fig. 3 XPS profile of HA, FHA and FHA/TiO_2 coatings. Inset upper left: narrow scan for F peak of FHA/TiO_2 composite coating; inset upper right: narrow scan for F peak of FHA coating. In the spectrum of HA coating, no F peak was detected

Table 2 F/Ca, Ca/P molar ratio and the theoretical molecular formulas of apatite crystals for all the coatings

	Ca/P	F/Ca	Theoretical formula
HA	1.61	–	$Ca_{10}(PO_4)_6(OH)_2$
FHA	1.62	0.125	$Ca_{10}(PO_4)_6(F_{1.25}OH_{0.75})$
FHA/TiO_2	1.64	0.125	$Ca_{10}(PO_4)_6(F_{1.25}OH_{0.75})$

apatite crystals with high purity were formed by this modified electrochemical deposition method. F content in FHA and FHA/TiO_2 composite coatings was similar suggesting that codeposition of TiO_2 particles did not interfere the formation of FHA.

The SEM observations of all the coatings after post-treatment are shown in Fig. 4a–f, respectively. The pure HA coating consisted of thin flakes which developed perpendicularly to the substrate (Fig. 4a). Adjacent curled flakes fused together on one joint to construct the micro-porous structure with pore diameter being about 1 μm. FHA coating appeared different in that it was composed of nano-scaled apatite crystals in particle-like appearance and nano-pores formed between those nano-crystals (<100 nm) (Fig. 4b). Two different features can be seen in the SEM micrograph of FHA/TiO_2 composite coating (Fig. 4c), the gray entangled and fused particles were FHA crystals and the small white particles were nanoscaled TiO_2, which were embedded uniformly between the FHA crystals. It can be seen that the average size of FHA crystals in the FHA/TiO_2 composite coatings was smaller than that in the pure FHA coating, indicating that the function of TiO_2 particles was to act as an FHA crystal grain growth inhibitor during electrochemical deposition. It was also found that the addition of TiO_2 particles caused a decrease in porosity and an increase in density of the composite coating. The less porosity and higher density may lead to higher cohesive strength of the coating, which was verified in the following bonding strength test. The cross-sectional morphologies of the coatings are shown in Fig. 4d–f. Smooth, uniform, approximately 5 μm thick layers were formed on the Ti substrates for all the coatings without delamination and/or cracks at the interface.

3.2 Process of electrochemical codeposition

Nanoscaled TiO_2 particles were codeposited with FHA on the Ti substrate after electrochemical codeposition, which can be seen in the SEM micrograph (Fig. 4c). This codeposition process may be attributed to the adsorption of TiO_2 on the cathode surface, as suggested by Guglielmi's two-step adsorption model [21]. Once the TiO_2 particles were adsorbed, FHA crystals began to build around the cathode slowly, encapsulating and incorporating the particles. Figure 5 shows the relationship between the

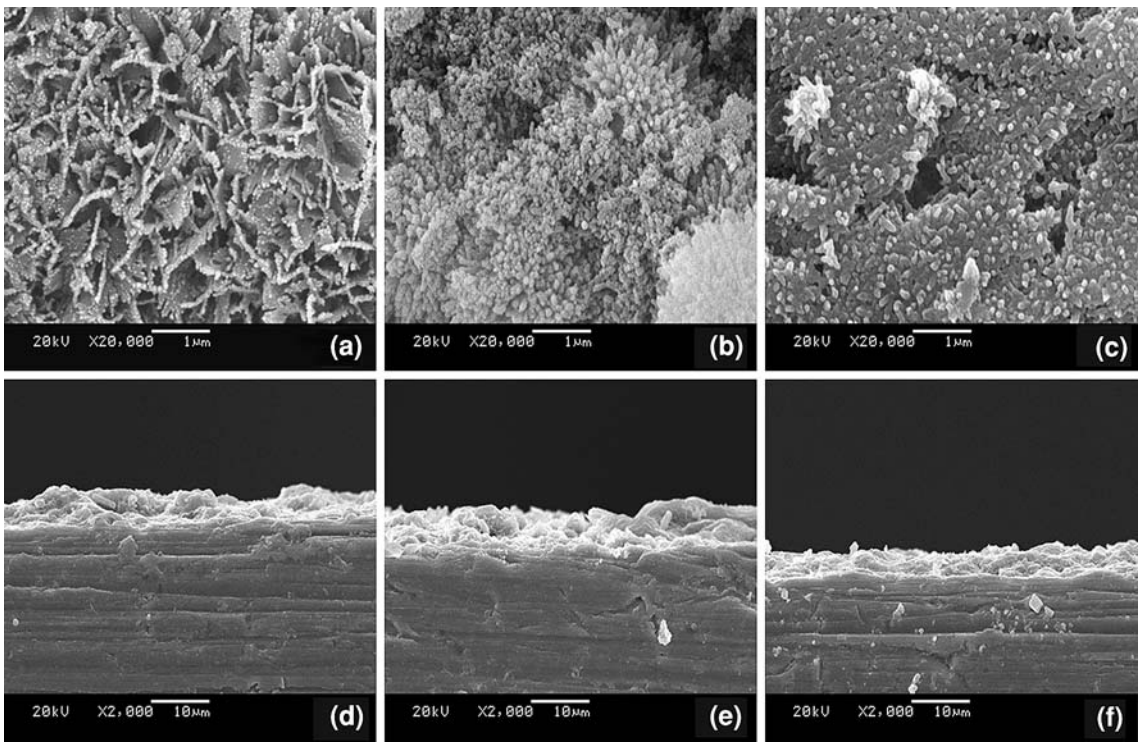

Fig. 4 SEM micrographs of apatite coatings after post treatment process. Suface morphologies: **a** HA coating, **b** FHA coating and **c** FHA/TiO_2 composite coating; cross-sectional morphologies: **d** HA coating, **e** FHA coating and **f** FHA/TiO_2 composite coating

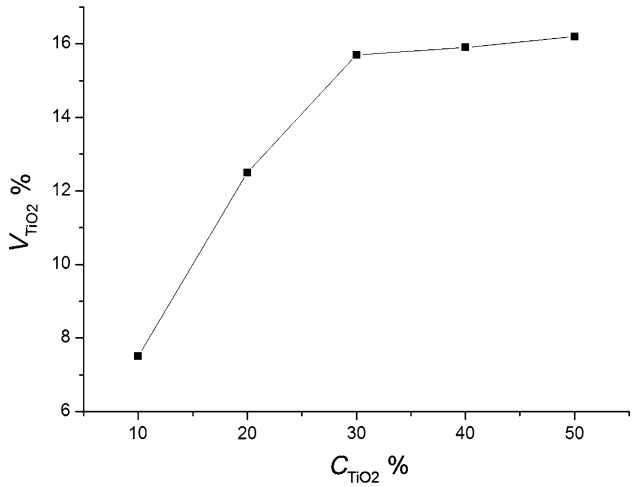

Fig. 5 Relationship between nanoscaled TiO_2 concentration in electrolyte and the content of TiO_2 in the composite coatings (*V*%)

concentration of TiO_2 particles in the electrolyte and the volume content of TiO_2 in the composite coatings (*V*%). It can be observed that TiO_2 in the coatings increased with an increase of TiO_2 in the electrolyte, tending to attain a steady value at TiO_2 concentration of 30 g/l. The curves were quite similar to the well known Langmuir adsorption isotherms, supporting a mechanism based on an adsorption effect. Therefore, the plateau observed at higher particles concentration in electrolyte may be a result of saturation in adsorption on substrate surface.

3.3 Bonding strength

The adhesion of the coatings was quantified by shear strength test following ASTM standard F1044-05 [22]. Although this test and its data analysis methodology are simple and there is an existing standard to follow, careful attention must be paid to the issue of bonding agent penetration. It is possible that the bonding agent (for example, epoxy resin) may penetrate through macropores or cracks in the film and partially bond to the substrate, thereby compromising the validity of the test result. In view of the issue of adhesive penetration, therefore, in the present study, the shear-fracture surfaces of the coated specimens were assessed by SEM and energy dispersive spectroscopy (EDS, Philips Series XL30) in order to ensure that epoxy resin did not penetrate the fracture surface. Those specimens with epoxy resin attached to the fracture surface were not included.

The bonding strength of the coatings with respect to the Ti substrate is shown in Fig. 6. The average bonding strength of pure HA coatings was 15.0 MPa after vacuum calcination and the values increased significantly to 21.5 and 26.3 MPa for FHA and FHA/TiO_2 coatings, respectively (ANOVA test, $P < 0.05$). The following conclusions

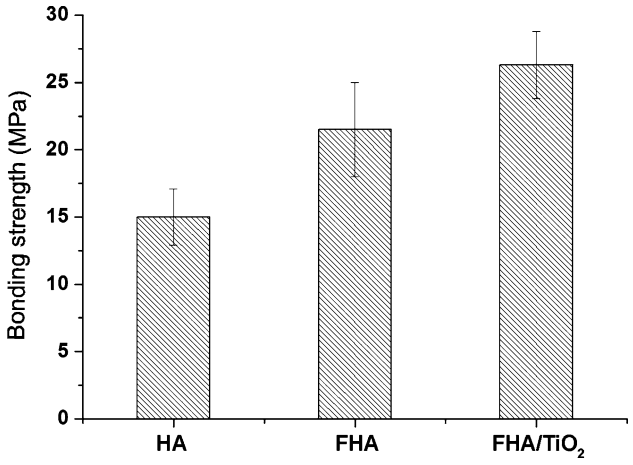

Fig. 6 Bonding strength of all the coatings with respect to Ti substrate

can be drawn from the measurements: (1) pure HA coating showed the lowest bonding strength; (2) the bonding strength of FHA coating was improved compared to HA coating, which can be understood by considering the

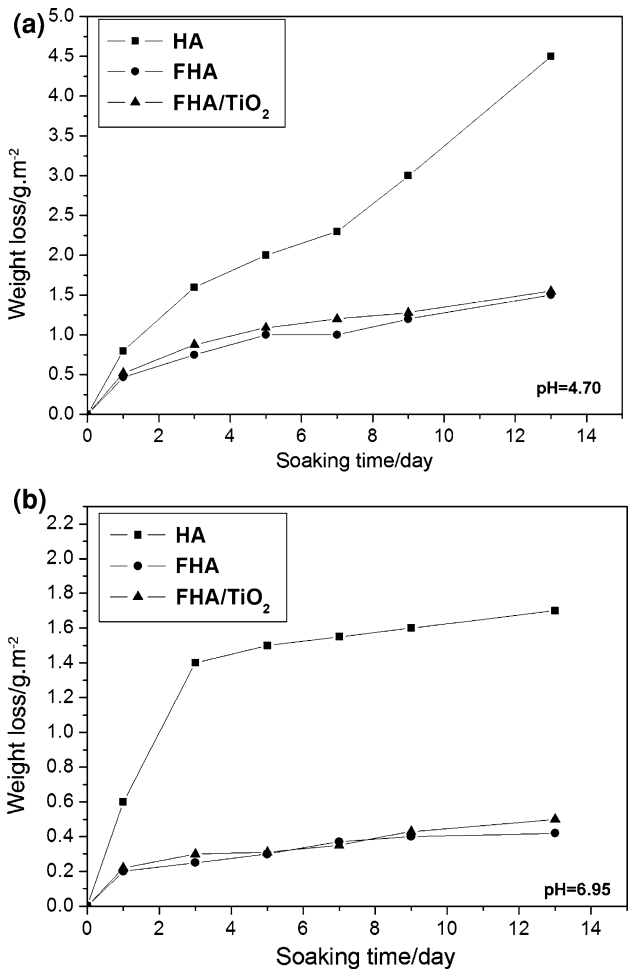

Fig. 7 Weight loss of the coatings against soaking time in CPBS with different pH values: (**a**) at 4.70 and (**b**) at 6.95

coefficient of thermal expansion (CTE) of the coatings. The incorporation of fluorine into apatite can decrease the CTE from 14×10^{-6}/°C for HA to 10×10^{-6}/°C for fluorapatite (the complete substitution of F for OH in HA) [27], therefore, the better bonding strength of FHA coating could arise from lesser thermal stress residue since the FHA coating has closer CTE to that of Ti (8.6×10^{-6}/°C) [28] than HA coating; and (3) the bonding strength of the composite coating was still higher than both HA and FHA coatings owing to several possible factors. First of all, the strengthening mechanism of HA/TiO_2 composite coating should relate to the dispersion strengthening by homogeneous distribution of TiO_2 particles in the coating. Other factors of microstructure, such as less porosity and smaller FHA crystal size certainly influenced the bonding strength of the composite coating. Furthermore, the favorable chemical affinity of TiO_2 with respect to FHA as well as to Ti substrate, i.e. its tight bonding to both FHA and Ti, greatly contributed to the observed improvement in bonding strength.

3.4 Dissolution behavior

Figure 7a, b show the dissolution behaviors of the coatings immersed in CPBS of different pH value (4.70 and 6.95), which was represented as the weight loss of them. It can be observed from the results that the dissolution amount depended on both soaking time and pH value of CPBS. HA coating had a larger dissolution amount than both FHA and FHA/TiO_2 coatings for any time and at any pH value. No significant difference in dissolution amount was detected between FHA and FHA/TiO_2 composite coating. Therefore, it can be assumed that apatite coatings incorporated with F^- ions had higher chemical stability than HA coating, which could be attributed to higher crystallinity and more compact apatite lattice structure.

3.5 Cellular responses

Figure 8a–d show typical SEM micrographs of MC3T3-E1 cells after 24 h of culture on HA coating, FHA coatings, FHA/TiO_2 composite coating and pure Ti substrate. As shown in Fig. 8a–c, the cells grew and spread well on all the coated specimens, suggesting that the coatings possess good cell viability. However, on the pure Ti surface (Fig. 8d), only a few cells could be seen within one microscope field and the cell density on Ti surface was much lower than that on coated specimens.

The in vitro cell compatibility was assessed by measuring the proliferation and ALP activity of MC3T3-E1 cells on all specimens after culturing for 7 days, with the results being displayed in Figs. 9 and 10, respectively. HA, FHA and FHA/TiO_2 coatings exhibited significantly higher cell proliferation and ALP activity as compared to pure Ti ($P < 0.05$), confirming the improved activity and functionality of cells on the substrate via the coatings.

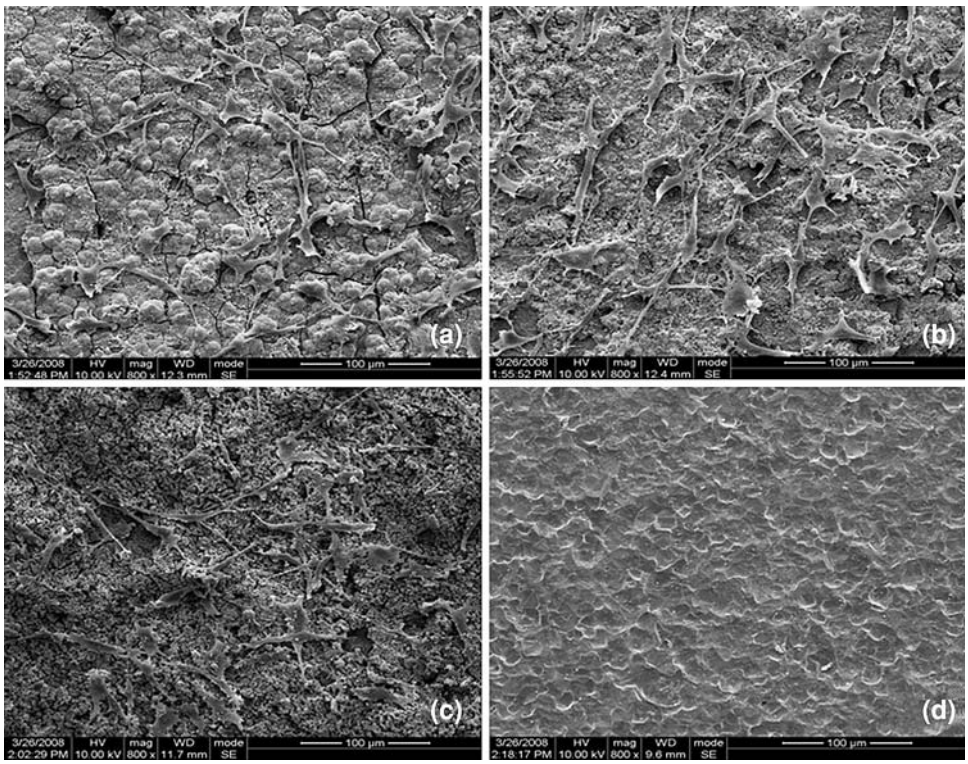

Fig. 8 SEM morphology of the MC3T3-E1 cells grown on **a** HA coating; **b** FHA coating; **c** FHA/TiO_2 composite coating and **d** pure Ti substrate

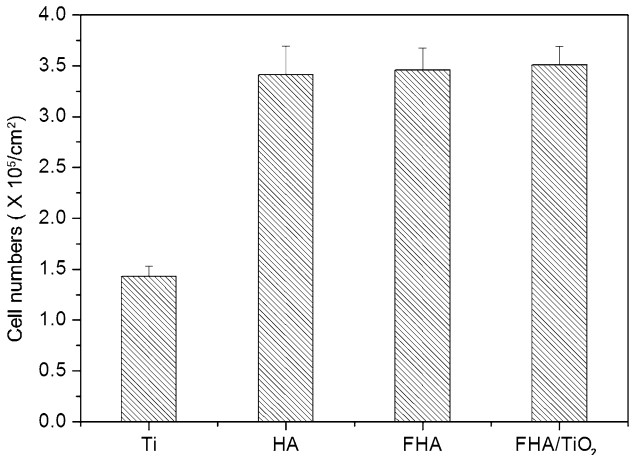

Fig. 9 Cell proliferation on the apatite coatings and titanium substrate after culturing for 7 days (ANOVA, $P < 0.05$). The cells on the coatings were detached with a trypsin-EDTA solution and the living cells were counted using a haemocytometer

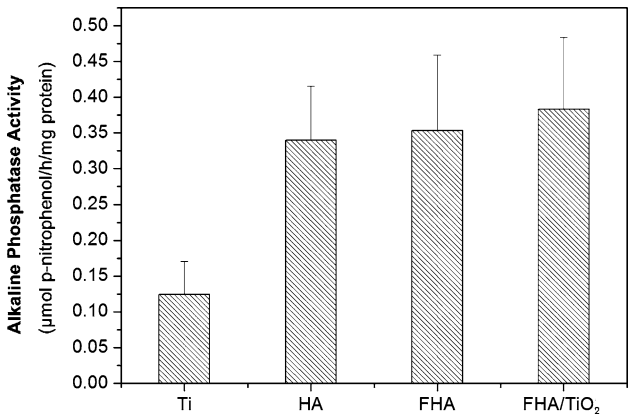

Fig. 10 ALP activity of MC3T3-E1 cells on apatite coatings and titanium substrate after culturing for 7 days (ANOVA, $P < 0.05$)

Meanwhile, no significant differences ($P > 0.05$) in both cell number and ALP activity were detected among HA, FHA and FHA/TiO_2 composite coating, which signified that the incorporation of either F^- ions or nanoscaled TiO_2 particles would not influence the bioactivity of HA coating.

4 Conclusions

A modified electrochemical technique was developed for co-depositing FHA/TiO_2 nanocomposite coating on the Ti substrate. Compared with HA coating, FHA/TiO_2 composite coating has higher crystallinity and lower grain size, indicating that the function of TiO_2 particles is to act as an FHA grain growth inhibitor. In addition, the composite coating showed higher bonding strength and lower dissolution rate than pure HA coating, and the in vitro bioactivity of FHA/TiO_2 composite coating was not affected when compared with pure HA coating. The present study shows that this electrochemical processing route may be a new direction for preparing a composite apatite coating that improves the physical and chemical properties of HA coating, without sacrificing the bioactivity.

Acknowledgements The authors thank Prof. Haiyang Yu, State Key Laboratory of Oral Diseases, Sichuan University for technical assistance in sample preparation. Tingting Liu, Department of orthodontics, West China College of Stomatology, Sichuan University, is acknowledged for the kind sharing of the MC3T3-E1 cells.

References

1. K. de Groot, R. Geesink, C.P.A.T. Klein, P. Serekian, J. Biomed. Mater. Res. **21**, 1375 (1987). doi:10.1002/jbm.820211203
2. L.L. Hench, J. Am. Ceram. Soc. **81**, 1705 (1998). doi:10.1111/j.1151-2916.1998.tb02540.x
3. H. Ji, C.B. Ponton, P.M. Marquis, J. Mater. Sci. Mater. Med. **3**, 283 (1992). doi:10.1007/BF00705294
4. S.R. Radin, P. Ducheyne, J. Mater. Sci. Mater. Med. **3**, 33 (1992). doi:10.1007/BF00702942
5. M. Shirkhanzadeh, J. Mater. Sci. Lett. **10**, 1415 (1991). doi:10.1007/BF00735695
6. M. Shirkhanzadeh, J. Mater. Sci. Mater. Med. **9**, 67 (1998). doi:10.1023/A:1008838813120
7. M. Kumar, H. Dasarathy, C. Riley, J. Biomed. Mater. Res. **45**, 302 (1999). doi:10.1002/(SICI)1097-4636(19990615)45:4<302:AID-JBM4>3.0.CO;2-A
8. M. Manso, C. Jimenez, C. Morant, P. Herrero, J. Martinez-Duart, Biomaterials **21**, 1755 (2000). doi:10.1016/S0142-9612(00)00061-2
9. L. Gineste, M. Gineste, X. Ranz, A. Ellefterion, A. Guilhem, N. Rouquet et al., J. Biomed. Mater. Res. B. **48**, 224 (1999). doi:10.1002/(SICI)1097-4636(1999)48:3<224::AID-JBM5>3.0.CO;2-A
10. S. Overgaard, M. Lind, K. Josephsen, A.B. Maunsbach, C. Bünger, K. Søballe, J. Biomed. Mater. Res. A **39**, 141 (1998). doi:10.1002/(SICI)1097-4636(199801)39:1<141::AID-JBM16>3.0.CO;2-I
11. J.S. Chen, H.Y. Juang, M.H. Hon, J. Mater. Sci.: Mater. Med. **9**, 297 (1998). doi:10.1023/A:1008825926440
12. X.F. Xiao, R.F. Liu, Y.Z. Zheng, Surf. Coat. Tech. **200**, 4406 (2006). doi:10.1016/j.surfcoat.2005.02.205
13. K. Cheng, W. Weng, U. Qu, P. Du, G.G. Shen, G. Han et al., J. Biomed. Matter. Res. B **69**, 33 (2004). doi:10.1002/jbm.b.20027
14. H.W. Kim, H.E. Kim, J.C. Knowles, Biomaterials **25**, 3351 (2004). doi:10.1016/j.biomaterials.2003.09.104
15. Y.Q. Zhai, K.Z. Li, H.J. Li, C. Wang, H. Liu, Mater. Chem. Phys. **106**, 22 (2007). doi:10.1016/j.matchemphys.2007.05.013
16. W. Suchanek, M. Yashima, M. Kakihana, M. Yoshimura, Biomaterials **18**, 923 (1997). doi:10.1016/S0142-9612(97)00019-7#
17. B. Labat, A. Chamson, J. Frey, J. Biomed. Mater. Res. **29**, 1397 (1995). doi:10.1002/jbm.820291111
18. H. Li, K.A. Khor, P. Cheang, Biomaterials **23**, 85 (2002). doi:10.1016/S0142-9612(01)00082-5#
19. Y.P. Lu, M.S. Li, S.T. Li, Z.G. Wang, R.F. Zhu, Biomaterials **25**, 4393 (2004). doi:10.1016/j.biomaterials.2003.10.092
20. P.A. Ramires, F. Cosentino, E. Milella, P. Torricelli, G. Giavaresi, R. Giardino, J. Mater. Sci. Mater. Med. **13**, 797 (2002). doi:10.1023/A:1016183326864

21. N. Guglielmi, J. Electrochem. Soc. **144**, 62 (1997)
22. ASTM Standard F 1044-05. (ASTM International, West Conshohocken, PA). doi: 10.1520/F1044-05
23. H.J. Robson, D.Q.M. Craig, D. Deutsch, Int. J. Pharm. **195**, 137 (1995). doi:10.1016/S0378-5173(99)00261-6
24. H.W. Kim, H.E. Kim, V. Salih, J.C. Knowles, J. Biomed. Mater. Res. A **68**, 522 (2004). doi:10.1002/jbm.a.20094
25. M. Cavalli, G. Gnappi, A. Montenero, D. Bersani, P.P. Lottici, S. Kaciulis et al., J. Mater. Sci. **36**, 3253 (2001). doi:10.1023/A:1017998722380
26. M.A. Stranick, M.J. Root, Colloids Surf. **55**, 137 (1991). doi:10.1016/0166-6622(91)80088-6
27. M.B. Bever, *Encyclopedia of materials science and engineering* (Pergamon, New York, 1986)
28. X.F. Xiao, R.F. Liu, Y.Z. Zheng, Mater. Lett. **59**, 1660 (2005). doi:10.1016/j.matlet.2005.01.037